Experiments in Fluids 38 (2005) 233–243
DOI 10.1007/s00348-004-0902-3

Analysis of interpolation schemes for image deformation methods in PIV

T. Astarita, G. Cardone

Abstract Image deformation methods in particle image velocimetry are becoming more and more accepted by the scientific community but some aspects have not been thoroughly investigated neither theoretically nor with the aid of simulations. A fundamental step in this type of algorithm is reconstruction of the deformed images that requires the use of an interpolation scheme. The aim of this paper is to examine the influence of this aspect on the accuracy of the PIV algorithm. The performance assessment has been conducted using synthetic images and the results show that both the systematic and total errors are strongly influenced by the interpolation scheme used in the reconstruction of the deformed images. Time performances and the influence of particle diameter are also analysed.

Abbreviations

BSPL *M*	interpolation scheme based on the B-spline of order *M*
FFT	fast Fourier transform
FFT *M*	interpolation scheme based on the shift theorem of the Fourier transform using *M* x *M* points
IDM	image deformation methods
IDWO	iterative discrete window offset
IS	interpolation scheme(s)
PID	particle image distortion
PIV	particle image velocimetry
SINC *M*	interpolation scheme based on the sinc formula using *M* x *M* points

List of symbols

D	particle diameter, pixels
f	grey intensity of the first image, dimensionless
g	grey intensity of the second image, dimensionless
i	horizontal image coordinate (integer value), pixels
j	vertical image coordinate (integer value), pixels
l	horizontal shift, pixels
m	vertical shift, pixels
N	number of measurement points, dimensionless
N_I	number of particles per interrogation window, dimensionless
$\boldsymbol{r}$	displacement field, pixels
$\boldsymbol{r}_c$	corrector displacement field, pixels
$\boldsymbol{r}_w$	displacement field averaged over the interrogation window, pixels
t	time needed to perform deformation of the images, seconds
$\bar{u}$	mean measured displacement, pixels
u	imposed displacement, pixels
u_i	local measured displacement, pixels
W	interrogation window linear dimension, pixels
x	horizontal image coordinate, pixels
y	vertical image coordinate, pixels
$\overline{\beta}$	mean bias error, pixels
β	bias error, pixels
$\overline{\sigma}$	mean total error, pixels
δ	total error, pixels
μ	mean operator
ϕ_{lm}	cross-correlation coefficient, dimensionless
σ	random error, pixels

Superscript

k	iteration counter, dimensionless

1 Introduction

Recently, particle image velocimetry (PIV) has become a widespread technique for measuring instantaneous flow fields and for this reason there is a great interest in the improvement of the technique. Clearly, continuous hardware evolution has an important effect in the bettering of PIV but, in the past few years, progress in digital analysis techniques has been surprising.

In the early 1990s various authors worked on an efficient digital approach to the analysis of PIV images and in most cases a classical cross-correlation approach was proposed, e.g. the works of Utami et al. (1991), Willert and Gharib (1991), Keane and Adrian (1993) and Westerweel (1993). By using this "classical" approach the "loss of pairs" (Keane and Adrian 1993) due to in-plane motion causes both a decrease of the signal-to-noise ratio and a significant increase of the total error, which is more evident for smaller particles.

Received: 16 July 2004 / Accepted: 13 October 2004
Published online: 22 December 2004

T. Astarita (✉), G. Cardone
University of Naples Federico II, DETEC, P. le Tecchio,
80–80125 Naples, Italy
E-mail: astarita@unina.it
Tel.: +39-081-7683389
Fax: +39-081-2390364

One of the possible solutions to this problem is to displace the interrogation windows by a discrete offset in order to follow the particles between the two different frames. Various authors have proposed an iterative discrete window offset (IDWO) approach and in particular the works by Soria (1996), Westerweel et al (1997), Scarano and Riethmuller (1999), Hart (2000) and Wereley and Meinhart (2001) are acknowledged.

The immediate extension of this method is the displacement of the interrogation windows by a "sub-pixel" offset (Lecordier et al. 2001). A further extension is to also take into account the deformation and rotation of the interrogation windows caused by the flow field. Huang et al. (1993) made pioneering work in this direction by introducing the particle image distortion (PID) technique. The main idea was to maximize the correlation coefficient in the presence of large velocity gradients. Deformation of the interrogation windows was evaluated by calculating the components of the velocity gradient and by applying classical kinematic formulae. Jambunathan et al. (1995) developed a different algorithm to estimate deformation of the interrogation windows. They simply interpolated the predictor displacement field on each pixel of the first image and used it to evaluate the distortion of the second image.

As also testified in a recent review article by Scarano (2002), image deformation methods (IDM) in PIV have recently became widely used and accepted. Use of this approach requires evaluation of the image intensity, also in location between the true pixels values and, consequently, an interpolation scheme (IS) must be used to reconstruct the images. To the authors' knowledge, in the literature there is not a systematic study of the effects of the interpolation schemes on the accuracy of IDM for PIV applications; thus, the aim of the present paper is to provide information on this aspect. The performance assessment is conducted using synthetic images with particles of Gaussian shape, a constant displacement field, and without added noise apart from the 8 bit digitalization. These hypotheses are clearly simplistic but the authors believe that many useful results and conclusion can still be drawn.

In Sect. 2 the PIV algorithm used in this work will be described in detail, while in Sect. 3 the experimental procedure and the synthetic image characteristics will be presented. In Sect. 4 the accuracy of classical (non IDM) methods will be analysed and compared, when possible, with previous results. In Sect. 5 various image interpolation schemes will be illustrated and in Sects. 6 and 7 their accuracy and time performances are presented. Prior to conclusions being drawn, Sect. 8 discusses an analysis of the influence of particle diameter on both the systematic and total error.

2 Iterative image deformation method

In the literature there are many contributions on IDM for PIV applications and, because each author propose a different approach, there is not a standard algorithm. Thus, this section illustrates in detail the iterative image deformation method used in this work, which is very similar to the one described by Scarano (2002). The algorithm is iterative and multigrid and the major steps are as follows:

1. The predictor displacement field is built with a standard cross-correlation method on a rather coarse grid. In particular, the FFT approach is used to evaluate the cross-correlation coefficient ϕ_{lm} between homologous square interrogation windows as:

$$\phi_{lm} = \frac{\sum_{i,j}^{W} \Big(f(i,j) - \mu_f\Big)\Big(g(i+l,j+m) - \mu_g\Big)}{\sqrt{\sum_{i,j}^{W} \Big(f(i,j) - \mu_f\Big)^2 \sum_{i,j}^{W} \Big(g(i,j) - \mu_g\Big)^2}} \qquad (1)$$

   where f and g are the grey intensities of the two interrogation windows extracted from the first and second image, μ_f and μ_g are the means evaluated over the corresponding interrogation windows, and W is the square window linear dimension. The use of FFT, for evaluation of the cross-correlation, produces a number of effects that are treated in detail by Raffel et al. (1998). The position of the maximum in the correlation plane is determined with subpixel accuracy by means of a three point Gaussian interpolation scheme (Westerweel 1993). Weighting factors can be used to correct the bias error associated with the imposed periodicity due to application of the FFT (Westerweel 1993; and Raffel et al. 1998). The displacement field obtained is then validated in order to remove possible outliers.
2. The predictor displacement field is interpolated on each pixel of the image by using a bilinear IS and, by using one of the interpolation schemes described in Sect. 5, the two complete images are deformed accordingly. This step is similar to the one proposed by Jambunathan et al. (1995) whereas the essential difference (apart from the IS) is that both images are distorted simultaneously (symmetrically). In this way it is possible to have a second order accurate estimation of the velocity (Nogueira et al. 1999; Wereley and Meinhart 2001).
3. A refinement may be performed resulting in the evaluation of the displacement field on a finer grid. Typically during the refinement process the linear dimension of the interrogation windows is halved, and in the final iterations, overlapping windows may be used.
4. Applying the method described in step 1 to the deformed images, a corrector displacement field is calculated.
5. To evaluate the true displacement field $\boldsymbol{r}(i,j)$ (for the sake of brevity, the dependence of $\boldsymbol{r}$ on the image coordinates will be dropped here) two courses of action may be pursued.[1] The first approach, proposed by Scarano (2004), is to sum the corrector displacement $\boldsymbol{r}_c$ with the displacement $\boldsymbol{r}_w$ obtained by averaging the predictor over the whole interrogation window:

[1] In many previous works this point is not described in detail, so it is difficult to clearly understand who was the first to propose the two approaches.

$$r^k = r_w^{k-1} + r_c^k \tag{2}$$

where the superscript indicates the iteration counter. This procedure enables a stable method even in the presence of high spatial frequencies (Scarano 2004). The second approach is to sum the corrector displacement with the local displacement obtained during the previous iteration:

$$r^k = r^{k-1} + r_c^k \tag{3}$$

As explained in detail by Nogueira et al. (1999), the latter method may be unstable if large spatial frequencies are present in the flowfield, thus an appropriate weighting of the interrogation windows should be used to avoid instabilities. Clearly this complicates the algorithm and does not add any further information to the influence of the interpolation schemes on the accuracy of IDM for PIV applications. For this reason, only the first approach will be used here. The obtained displacement field is then used as a predictor for step 2.

Steps 2–5 are repeated for a prescribed number of times. Typically three iterations are needed to reach the final dimensions of the interrogation windows and then one or two iterations at the final overlapping factor are needed to reach convergence.

3 Procedure

Synthetic images are used to estimate the influence of different IS on the accuracy of iterative image deformation methods for PIV application and only constant (along a principal direction) displacement fields are simulated. Each particle is supposed to be of Gaussian shape and thus the intensity level is obtained by integrating the particle light distribution over each image pixel. The latter supposed to have a unity fill factor and a maximum level of 255, i.e. 8 bits. If two or more particles overlap, the intensity level of each pixel is the sum of the intensities relative to each particle. In most of the simulations a standard set of images is used, in this case, a sample of 81 images with a constant displacement linearly varying between 0 and 4 pixels (i.e. a step of 0.05 pixels) and about 20 thousands particles randomly distributed are generated in a 512×512 pixels image resulting in a particle density of 0.076 particles per square pixel. A uniform randomly varying particle mean diameter D of 3 pixels with a maximum deviation of ±0.5 pixel and mean brightness of 120 with a maximum deviation of ±40 is also used. No additional noise is used because only the influence of the interpolation schemes on the accuracy of IDM for PIV applications is investigated.

Since the exact displacement field is known it is possible to easily define three types of errors: bias β, random σ and total δ (Gui and Wereley 2002):

$$\beta = u - \overline{u} \tag{4}$$

$$\sigma = \sqrt{\frac{1}{N}\sum_{i=1}^{N}(u_i - \overline{u})^2} \tag{5}$$

$$\delta = \sqrt{\frac{1}{N}\sum_{i=1}^{N}(u_i - u)^2} \tag{6}$$

where $\overline{u}$ is the mean measured value, u is the exact imposed displacement, u_i the measured displacement and N is the number of samples. Clearly, the three errors satisfy the equation $\delta^2 = \sigma^2 + \beta^2$.

In this work the bias error and the total error will be shown and most of the results will be presented for a final interrogation window of 16×16 pixels. The number of samples used for computation of the bias and total errors is always greater than 14 thousand.

4 Accuracy of classical methods

First of all the accuracy of the classical cross-correlation method will be analysed and compared with the results obtained by Raffel et al. (1998). Such a comparison is shown in Fig. 1 where, for three different values of the number of particles per interrogation window N_I, W =32, D =2.2 and a fixed brightness of 120 (i.e. practically the same conditions of Raffel et al. 1998), δ is plotted against the imposed displacement u. Open symbols are relative to the data of Raffel et al. (1998) while closed ones to the present simulations. The error increases almost linearly with the imposed displacement and decreases with increasing particle density; this agreement should confirm the goodness of the procedure.

By using the standard set of images, the comparison between IDWO methods and the classical cross-correlation approach (circles are used as symbols) is shown in Fig. 2. In particular, both the symmetric (diamonds) and asymmetric (triangles) displacement window offset is used. To show the effects of the correction on the bias error associated with the imposed periodicity (see Sect. 2, point 1), open symbols are used for corrected values while closed ones for the raw data. By looking at Fig. 2a where β is plotted, it is possible to see that, for both the corrected and raw data, the bias error is equal for the three methods untill the displacement is less than 0.5 pixels, i.e. while the

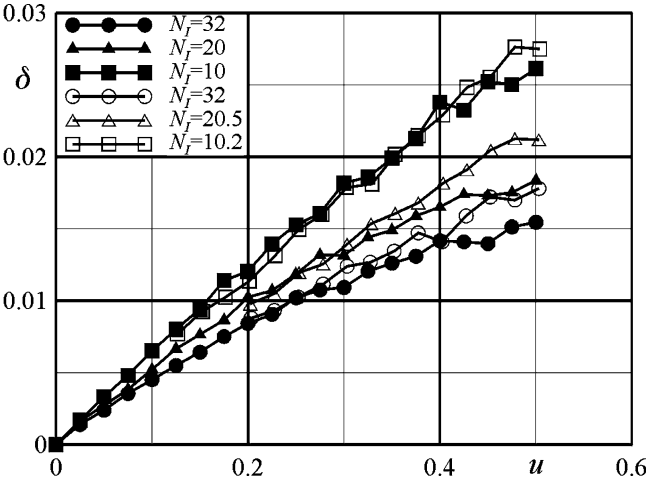

Fig. 1. Total error as a function of the imposed displacement for different N_I values; closed symbols are relative to present data while open ones to data of Raffel et al. (1998)

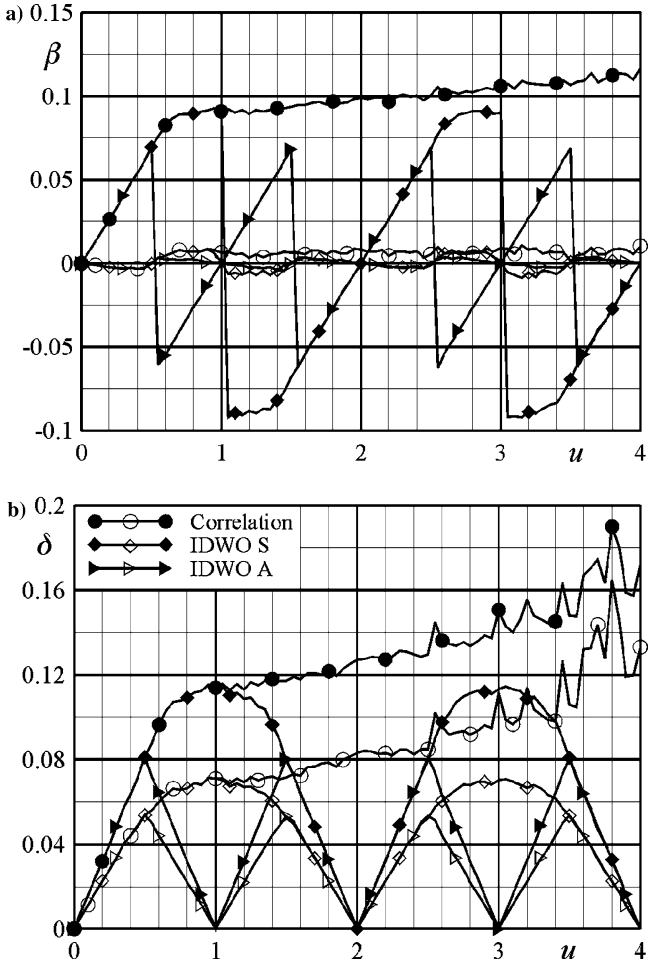

Fig. 2. Bias (**a**) and total (**b**) errors as a function of the imposed displacement for the classical algorithms; open symbols are relative to corrected values while closed ones to raw data

two IDWO methods and the classical cross-correlation approach are equivalent. The raw data show a significant bias error that is more than one order of magnitude higher than the corrected one.

By focusing attention on the raw data it is evident that both the IDWO methods show a periodic behaviour for β with a period equal to 1 or 2 pixels for the asymmetric and symmetric methods, respectively. Indeed, for the former method, the interrogation windows in the second image are offset by 1 pixel when the predictor displacement is greater than 0.5 pixels and by two pixels when the displacement reaches 1.5 pixels, and so on. For the symmetric method both the interrogation windows, in the first and second image, are offset by 1 pixel when the displacement is greater than 1 pixel and by two pixels when the displacement reaches 3 pixels, and so on. The periodic behaviour is typical of iterative methods and will be found again for the image deformation methods. Since the symmetric method follows the classical cross-correlation methods for a larger imposed displacement its bias error is, on average, larger with respect to the asymmetric one. The comparison of the present results with the ones of Scarano and Riethmuller (2000) and of Gui and Wereley (2002) is fairly good even if in both cases β is slightly higher than the present values. The latter authors used 32×32 interrogation windows and synthetic images with particles that, on average, have a diameter slightly larger than the one used in the present work and this latter effect might explain the small discrepancy. Even if not clearly stated, it is probable that the authors of both the cited papers did not use the correction for the bias error and used an asymmetric IDWO method. When the correction associated with the imposed periodicity of the interrogation windows is applied, the bias error shows, for the classical cross-correlation approach, a change of sign for $u < 0.5$ and then reaches a nearly constant value.

The graph of Fig. 2b show a similar behaviour for δ. The total error for the raw data, similar to that found by Scarano and Riethmuller (2000), is significantly higher relative to the curves obtained by applying the correction on the bias error associated with the imposed periodicity of the interrogation windows. The classical cross-correlation method shows a large oscillation of δ for $u > 3$ pixels which is due to the loss of pairs associated with the large imposed displacement. Clearly the iterative nature of the two IDWO methods completely removes this type of random error and, for this reason, only data relative to $u < 2$ pixels will be further presented herein.

5
Image interpolation schemes for PIV

As it will be seen in the next section the choice of the interpolation scheme is of fundamental importance in the application of IDM and for this reason various IS will be analysed. The well known bilinear interpolation scheme is widely used in PIV algorithms, for example, it can be found in the works of Huang et al. (1993), Jambunathan et al. (1995), Nogueira et al. (1999), Gui and Wereley (2002), and Meunier and Leweke (2003). The bilinear interpolation formula may be easily found by using successive linear interpolations along the two principal directions. First, two intermediate values are evaluated by means of linear interpolations along the x direction (a sample interpolation grid, also called stencil in the following, is shown in Fig. 3a):

$$f_{x,y=0} = f_{0,0} + x\left(f_{1,0} - f_{0,0}\right) \tag{7}$$

$$f_{x,y=1} = f_{0,1} + x\left(f_{1,1} - f_{0,1}\right) \tag{8}$$

where, for the sake of brevity but without loss of generality, it is assumed that both x and y are included in the interval [0 1], and the image coordinates are indicated by subscripts.

The obtained values are then interpolated along the y direction:

$$\begin{aligned} f_{x,y} &= f_{x,y=0} + y\left(f_{x,y=1} - f_{x,y=0}\right) \\ &= (1-x)(1-y)f_{0,0} + x(1-y)f_{1,0} + (1-x)yf_{0,1} + xyf_{1,1} \end{aligned} \tag{9}$$

Equation 9 is the standard bilinear formula. By using the same procedure it is possible to find IS of higher order, e.g. by using three quadratic interpolations along the x direction and a successive quadratic interpolation along

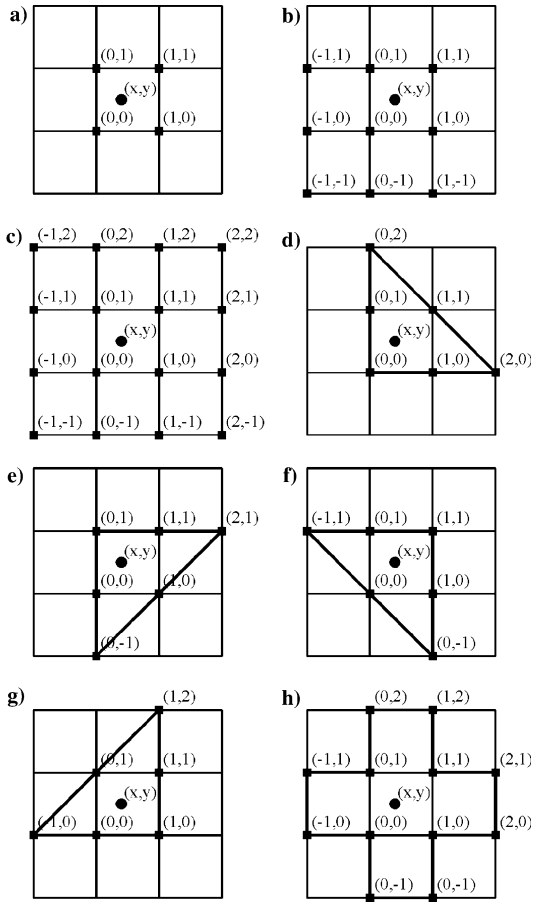

Fig. 3. Interpolation grids for various IS. **a** Bilinear. **b** Biquadratic. **c** Bicubic. **d–h** Simplex

the y direction the biquadratic interpolation formula can be found. The biquadratic interpolation formula, used by Nogueira et al. (2001) for PIV application, should be more accurate because it uses information from nine neighbouring points as shown in the grid of Fig. 3b. The successive approximation is the bicubic interpolation that uses the information from 16 neighbouring points (Fig. 3c).

Another family of IS is based on a simplex stencil that results in three points for the linear approximation, six for the quadratic, and so on for increasing order. From Fig. 3d–g, which shows, for the quadratic simplex IS, the four possible interpolation grids each rotated 90° with respect to the previous one, the lack of symmetry of this scheme is clear. A possible way to overcome this problem is to average the values of the interpolations from the four different simplexes; in this way 12 points are used for the final formula (Fig. 3h):

$$\begin{aligned} f_{x,y} = {} & f_{0,0} + \frac{x^2}{8}\left(+f_{0,-1} - f_{0,0} - f_{0,1} + f_{0,2} + f_{1,-1} - f_{1,0} - f_{1,1} + f_{1,2}\right) \\ & + \frac{y^2}{8}\left(f_{-1,0} + f_{-1,1} - f_{0,0} - f_{0,1} - f_{1,0} - f_{1,1} + f_{2,0} + f_{2,1}\right) \\ & + xy\left(f_{0,0} - f_{0,1} - f_{1,0} + f_{1,1}\right) \\ & + \frac{x}{8}\left(-f_{0,-1} - 7f_{0,0} + 9f_{0,1} - f_{0,2} - f_{1,-1} + f_{1,0} + f_{1,1} - f_{1,2}\right) \\ & + \frac{y}{8}\left(-f_{-1,0} - f_{-1,1} - 7f_{0,0} + f_{0,1} + 9f_{1,0} + f_{1,1} - f_{2,0} - f_{2,1}\right) \end{aligned} \tag{10}$$

Scarano and Riethmuller (2000) suggest using an interpolation scheme based on the sinc function (it will be further referred to here as SINC IS):

$$f_{x,y} = \sum_{i=-\infty}^{i=\infty} \sum_{j=-\infty}^{j=\infty} f_{i,j} \frac{\sin \pi(i-x)}{\pi(i-x)} \frac{\sin \pi(j-x)}{\pi(j-x)} \tag{11}$$

Furthermore, they suggest using an interpolation grid of 7×7 pixels. A similar formula may be obtained by applying the well known shift theorem of the Fourier transform in the frequency domain (here referred to as FFT IS). A discussion on the characteristics of these last two interpolation schemes and their relationships can be found in a paper by Yaroslavsky (1996). As the number of points used in these types of IS may be chosen arbitrarily, in the following the number that follows the acronym will indicate the linear dimension of the interpolation grid, e.g. FFT3 indicates the Fourier shift theorem IS on a grid of 3×3 points.

The last family of interpolation schemes used in this work is the one based on B-spline functions (BSPL). In this case it is also possible to use square interpolation grids with a linear dimension that is a function of the spline order. In particular, a spline of order two uses a stencil of 3×3 points, while a spline of order three uses 4×4 points. By slightly changing the convention introduced in the previous paragraph, the number following the acronym will indicate the order of the B-spline and not the stencil linear dimension. Details on implementation of the algorithm and on the relations of the B-spline IS with the cardinal interpolation formula can be found in Unser et al. (1993a, 1993b) and in Unser (1999).

Clearly it is expected that if more points are used for the IS the accuracy should improve while the time performance should worsen. As will be seen this is not always the real situation and other factors, like the choice of odd or even linear dimensions of the interpolation grid, may produce different behaviours of the interpolation schemes in the PIV process.

6
Accuracy of image deformation methods

Each interpolation scheme described in the previous section will now be analysed in detail. A comparison of the "high speed" IS, i.e. the ones that use 16 or less points, is shown in Fig. 4a and b; the curves relative to the symmetric IDWO method (diamonds) are also included for reference. In this figure the correction on the bias error associated with the imposed periodicity has been applied and the same images of section 4 are processed. By looking at Fig. 4b, where the total error is plotted, it is clear that the worst results are those relative to the FFT3 (triangles) and biquadratic IS (stars) both of which have odd linear dimensions of the interpolation grid. A significant part of the total error is due to the extremely high bias error, for this reason in Fig. 4a the two curves relative to the aforementioned IS are not plotted. It is interesting to note that for these two IS the total error can be even larger relative to the classical cross-correlation method and a period of two pixels is found. The bilinear IS (open

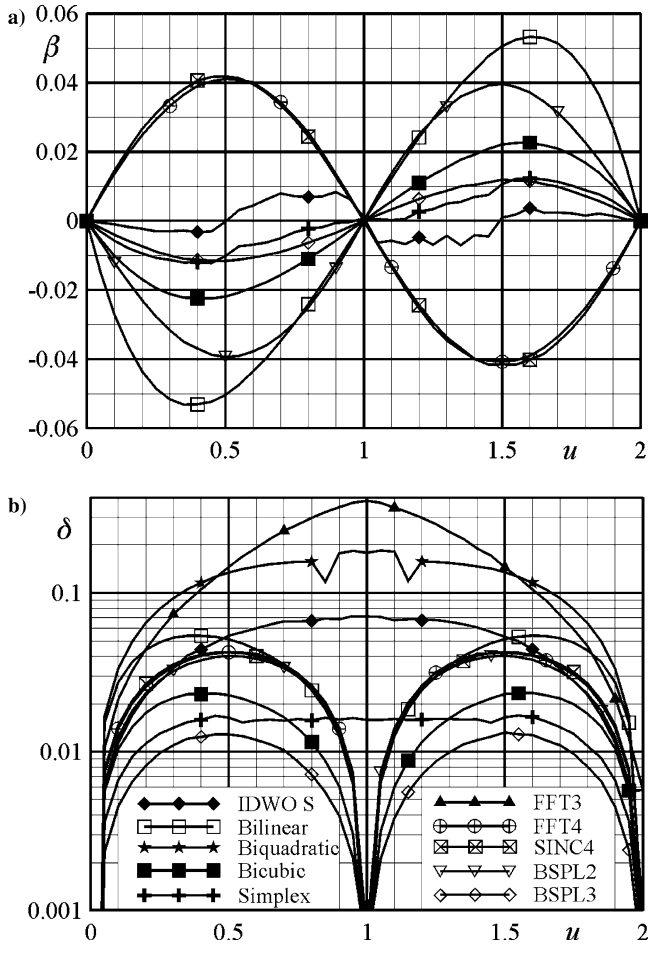

Fig. 4. Bias (**a**) and total (**b**) errors as a function of the imposed displacement for various IS

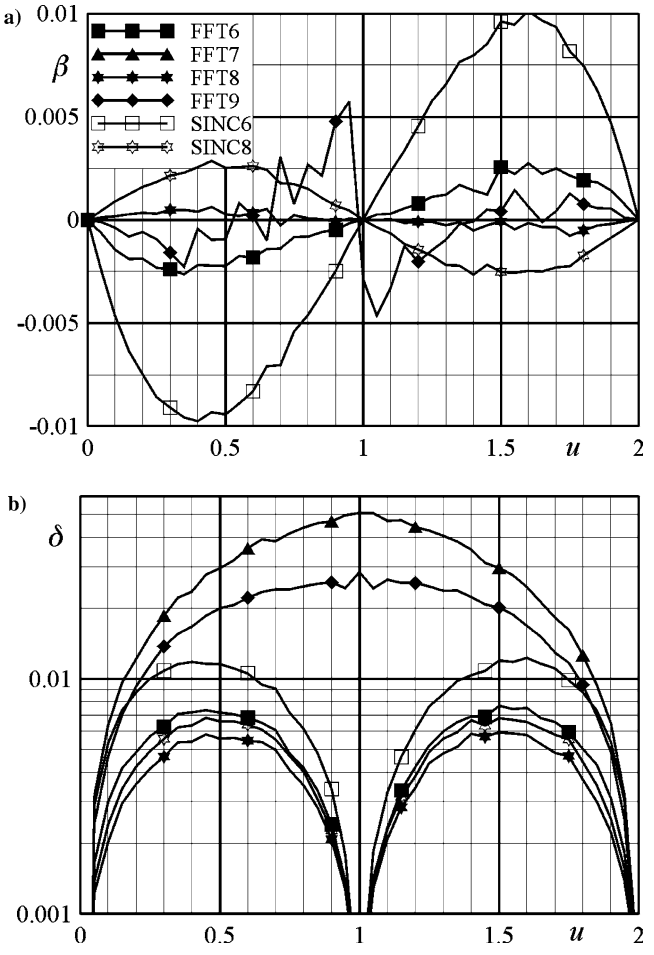

Fig. 5. Bias (**a**) and total (**b**) errors as a function of the imposed displacement for various IS

squares) performs relatively well considering the small number of points used. Even if the IDM used in this paper is symmetric, and should have a period of two pixels, this IS has a period of one pixel for the total error which reduces significantly the average total error. A similar behaviour, but with a slightly smaller error, is seen for the FFT4 (crossed circles), SINC4 (crossed squares) and BSPL2 IS (open triangles) and it is clear that the differences between them, in this case, are very small. The bicubic formula (closed squares) performs significantly better by halving the error with respect to the bilinear IS. The simplex IS (open crosses) behaves even better and has a flatter response with a period of two pixels. The BSPL3 (open diamonds) attains, among the high speed interpolation schemes, the smaller total error again with a periodic behaviour and a period of one pixel. Apart from the first two IS, the IDM has an average total error smaller than that relative to the symmetric IDWO method (closed diamonds) but the same is not true for the bias error. In Fig. 4a it is clear that the smaller bias error is obtained by using the classical IDWO method while the IDM may have significantly higher errors. In particular, the larger systematic error is associated with the bilinear interpolation scheme, followed by FFT4, SINC4 and BSPL2 IS. Bicubic, BSPL3 and simplex interpolation schemes again perform better. For all the IDM the period is two pixels and β is equal to zero for integer displacements.

Present data for the bilinear IS should be, in principle, comparable with the results of Gui and Wereley (2002), but comparison of the bias error is unsatisfactory which is most probably due to the fact that, in the present case, smaller interrogation windows are used and both the images are deformed symmetrically while, most probably, in their case the asymmetric approach has been followed. This should explain both the halved period of their data and the smaller error. In particular the latter effect is also due to the fact that one image is not reconstructed, thus reducing the interpolation errors. Clearly, as previously stated, by distorting symmetrically both the images it is possible to have a second order accurate estimation of the velocity when the displacement is not constant.

The effects of varying the linear dimension of the interpolation grid for the Fourier shift theorem interpolation formula and the SINC IS are shown in Figs. 5 and 6. In particular the total error for the FFT IS for an interpolation grid from 6x6 to 9×9 and for the SINC IS with a stencil of 6×6 and 8×8 is plotted as a function of the imposed displacement in Fig. 5b. In Fig. 6b only even stencil from 10×10 to 16×16 points are shown. Closed symbols refer to the FFT IS and open symbols to the SINC IS. As already observed, when the linear dimension of the

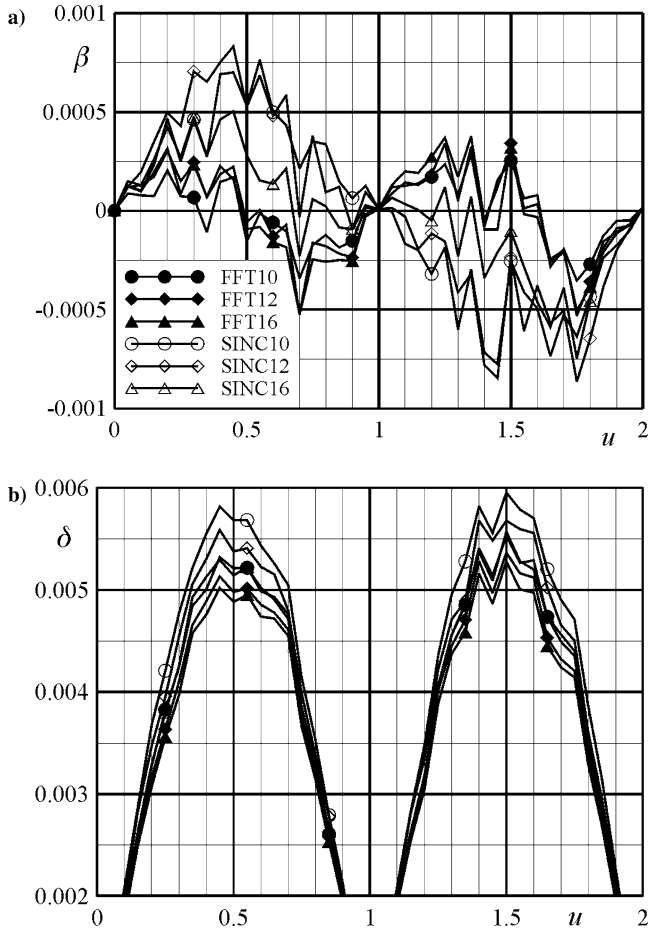

Fig. 6. Bias (**a**) and total (**b**) errors as a function of the imposed displacement for various IS

interpolation grid is odd this IS behaves poorer with a period of two pixels. Similarly for the total error, and even when using 9×9=81 points, the total error is higher than that relative to the simplex method (Fig. 4b). Results relative to the FFT7 interpolation scheme differ significantly from the data of Scarano and Riethmuller (2000) both in magnitude and in shape. Most probably this discrepancy is analogous to the one with the data of Gui and Wereley (2002). The behaviour is completely different for an even number of points on the interpolation grid's linear dimension, the period is again one pixel and the maximum total error for the FFT IS on 8×8 points, in this case, decreases by a factor of two with respect to the BSPL3; some smaller effects are achievable with a bigger stencil (Fig. 6b). For an even linear dimension of the stencil the Fourier shift theorem based interpolation schemes behave a little better with respect to the SINC IS. The bias error follows a similar behaviour, as shown by Figs. 5a and 6a, reaching for an odd linear dimension of the stencil higher values with respect to even ones. In particular, the curve relative to the FFT7 IS has not been plotted on account of its large bias error. Increasing the linear dimension of the interpolation grid, β decreases considerably reaching values that are one order of magnitude smaller than that relative to the classical methods (less than 0.0005 pixels for the FFT based interpolation schemes).

The effects of varying the dimensions of the interpolation grid for the B-spline interpolation scheme are shown in Fig. 7. As seen in Fig. 7a, where the bias error is plotted, increasing the stencil dimension β decreases significantly at first and then only slightly. In particular for the bigger interpolation grid the bias error reaches values that are very similar to the ones relative to the FFT and SINC interpolation schemes. The total error, shown in Fig. 7b, is less influenced by the stencil dimension and practically does not change for B-spline of order seven or higher. It is interesting to note that the BSPL interpolation scheme is not influenced by a choice of odd or even linear dimension of the interpolation grid and the error is monotonically decreasing with the spline order.

Figure 8 shows the curves relative to the same IS of Fig. 4 but without the correction of the bias error associated with the imposed periodicity of the interrogation windows. As expected the only curve that is significantly affected by the correction is that relative to the IDWO method; the iterative nature of IDM methods completely removes the need for the bias correction because at each iteration the relative displacement decreases and with it the bias error. Unexpectedly, in some cases, both the total and bias error tend to slightly decrease for IDM by neglecting the bias correction but the overall behaviour does not change.

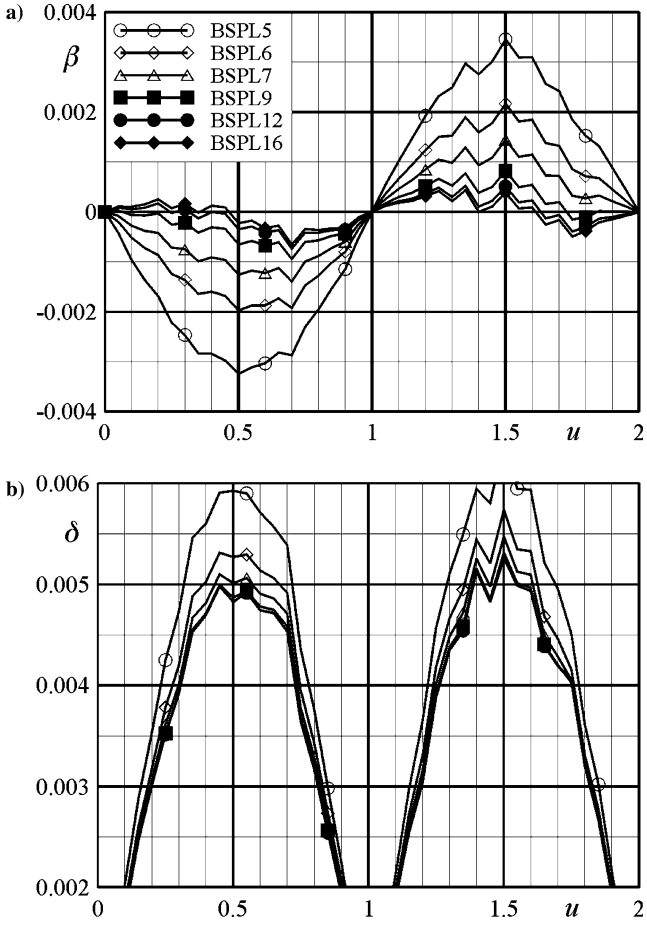

Fig. 7. Bias (**a**) and total (**b**) errors as a function of the imposed displacement for various IS

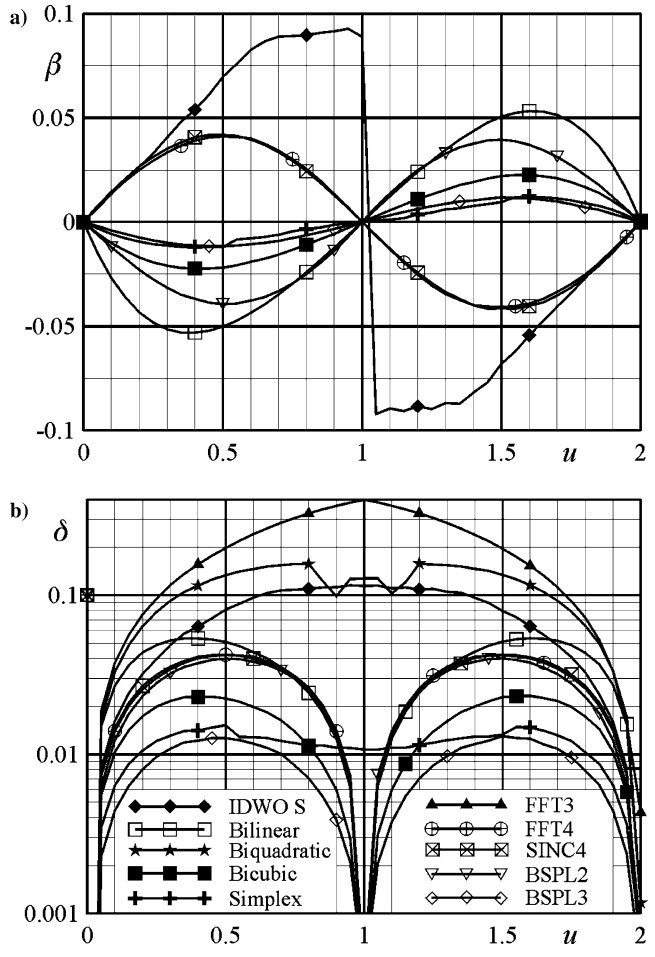

Fig. 8. Bias (**a**) and total (**b**) errors as a function of the imposed displacement for various IS

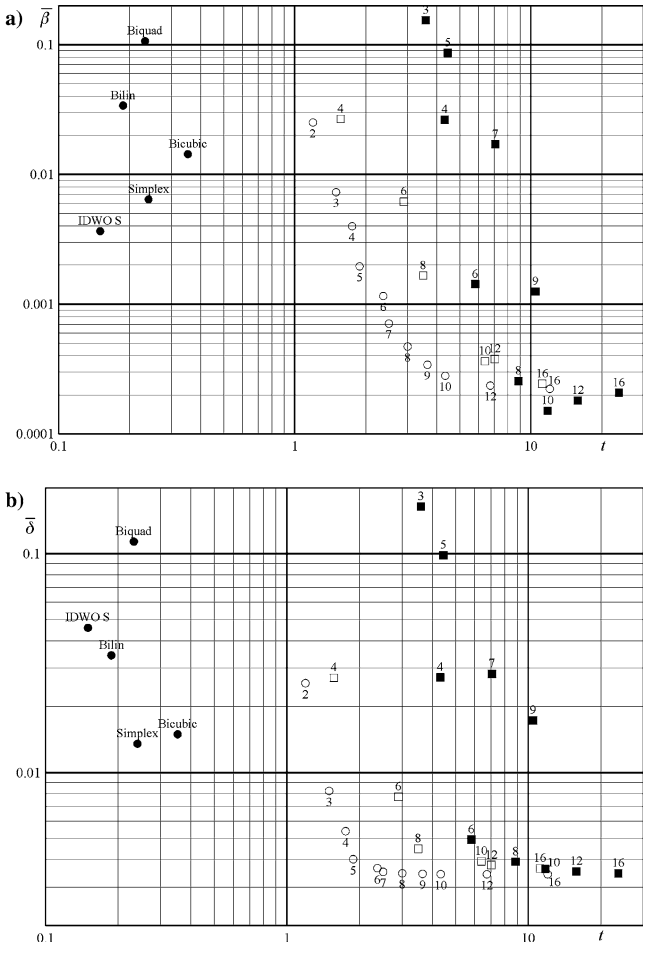

Fig. 9. Bias (**a**) and total (**b**) mean errors as a function of time for various IS. *Closed circles* indicate high speed methods, *open circles* BSPL IS (the number indicates the spline order), *closed squares* and *open squares* FFT and SINC interpolation schemes (the number indicates the stencil linear dimension), respectively

7
Time performance of image deformation methods

For processing large amounts of PIV images both high accuracy and low processing times are needed. For this reason, in Fig. 9a and b, the mean bias and total errors for the standard images, evaluated by averaging the absolute value of the errors in the displacement interval from zero to four pixels, are plotted against the time t needed to deform the images (i.e step 2 of Sect. 2).[2] For the classical method t is equal to zero and so the abscissa for this point has been fictitiously fixed at 0.15 s. Closed circles indicate high speed methods, open circles BSPL IS (the number indicates the spline order), closed squares and open squares FFT and SINC interpolation schemes (the number indicates the stencil linear dimension), respectively.

By focusing attention on the high speed methods it is evident that the time needed to perform the image deformation does not change much while both the total and bias error may change considerably. The total error for the simplex and bicubic interpolation schemes is significantly smaller than that relative to the symmetric IDWO method but the biquadratic IS performs worse. The average bias error is smaller for the classical method.

[2] Of course the time t is a function of the computer used during the simulation so it should be regarded as a relative measurement.

By using BSPL, FFT or SINC interpolation schemes on rather big interpolation grids, the performances of IDM change radically. The time needed to deform the images may increase more than one order of magnitude while both the errors decrease significantly. The FFT methods are slower than SINC and BSPL interpolation schemes. The BSPL IS has the advantage of reducing significantly the total error, also for smaller interpolation grids. For big interpolation grids, i.e. 16×16 points, both the bias and the total error result one order of magnitude smaller than that relative to the IDWO method.

8
Influence of the particle diameter

It is well known that the particle diameter influences significantly the performance of the PIV algorithm. Westerweel (2000) has analysed this effect both theoretically and by using synthetic images for the classical methods and found, in agreement with the simulation of Raffel et al. (1998), that the optimal particle diameter is of about two pixels, i.e. rather small. In this section the influence of particle diameter on the accuracy of IDM methods will be analysed. A set of 96 synthetic images is used with a fixed

particle diameter ranging from 0.5 to 10 pixels and the same particle density of the standard set of images. Following the same symbology of Figs. 4, 5 and 6, the total and bias error for a fixed imposed displacement of 1.5 pixels are shown in Figs. 10, 11 and 12.

As seen in Fig. 10b—although the same also occurs for bigger stencils—most of the curves tend to overlap for high values of particle diameter which is most probably due to the small number of points (5) used in interpolation of the correlation map maximum. The optimal particle diameter for the classical IDWO method is found to be of about two pixels, which is in perfect agreement with the cited papers. As already found, the FFT3 IS performs poorly for all the tested particle diameters. The biquadratic, bilinear, BSPL2, bicubic and BSPL3 IS, in this order, perform increasingly better and have a larger optimal particle diameter. The SINC4 has a relatively large plateau where the total error attains a minimum. The FFT4 has an optimal particle diameter of about two pixels and for small D performs better than the other methods. The simplex method has an optimal diameter of about four pixels. As shown in Fig. 10a the bias error for most of the interpolation schemes is higher, for all the tested particle diameters, with respect to the classical IDWO method. Comparison with data presented by Gui and Wereley (2002) is quite good and the δ profiles, for both the IDWO

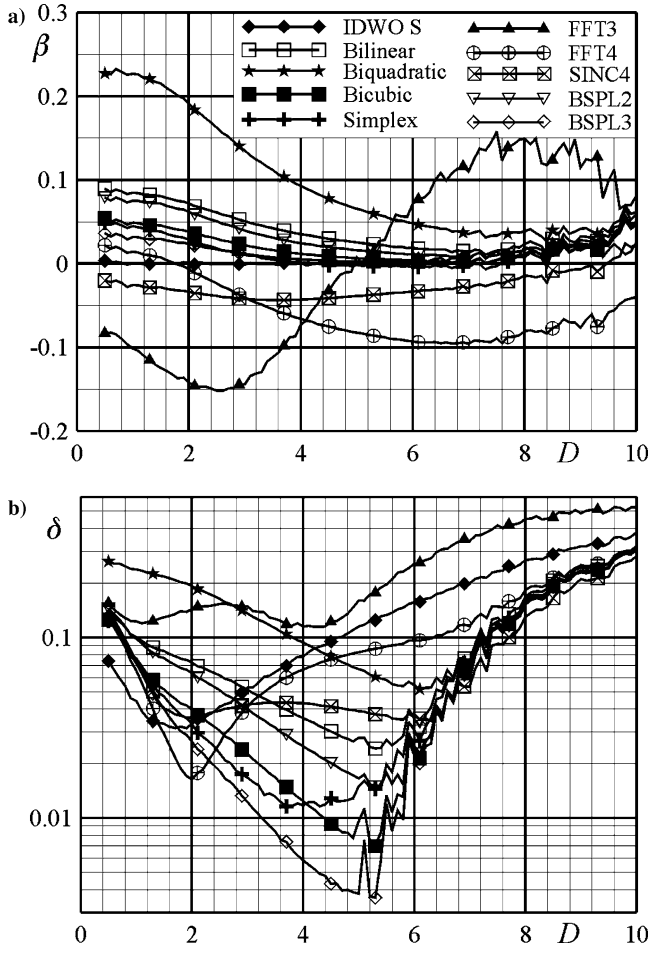

Fig. 10. Bias (**a**) and total (**b**) errors as a function of particle diameter for various IS

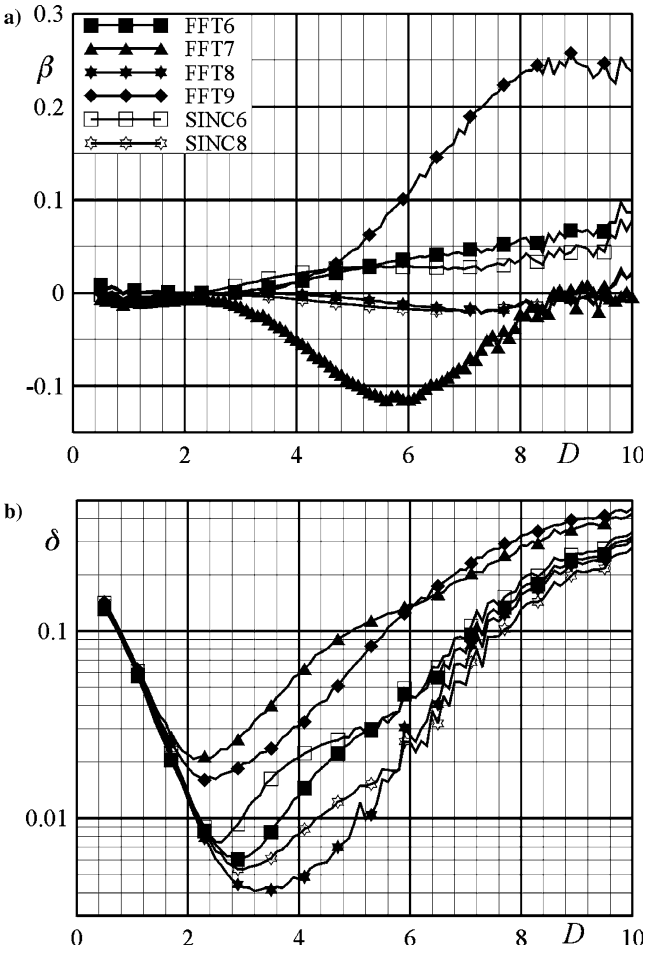

Fig. 11. Bias (**a**) and total (**b**) errors as a function of particle diameter for various IS

and bilinear IS, resemble the ones reported herein. In particular the previous authors did not find the absolute minimum for the bilinear interpolation scheme because they tested particle diameters of maximum 5 pixels.

Figure 11 shows the curves relative to the same IS shown in Fig. 5. Again, the methods based on odd linear dimensions perform poorly with regard to both the total and bias error. From Fig. 11b it is evident that for small particle diameters all the curves behave in the same way but the absolute minimum tends to shift to higher D with increasing linear dimension of the interpolation grid. In Fig. 12b a similar behaviour is also found for larger stencils but in this case a relatively large plateau is found. The bias error appears to increase significantly when the particle diameter is bigger than the value relative to the minimum for the total error. For bigger interpolation grids the B-spline interpolation scheme has a behaviour that is very similar to the FFT IS. From Fig. 13, where δ and β for the FFT16 (thick grey line) and BSPL16 (thin black line) IS are plotted, it is evident that the two IS schemes are practically equivalent.

9 Conclusions

The influence of the interpolation schemes on the accuracy of image deformation methods for PIV applications has

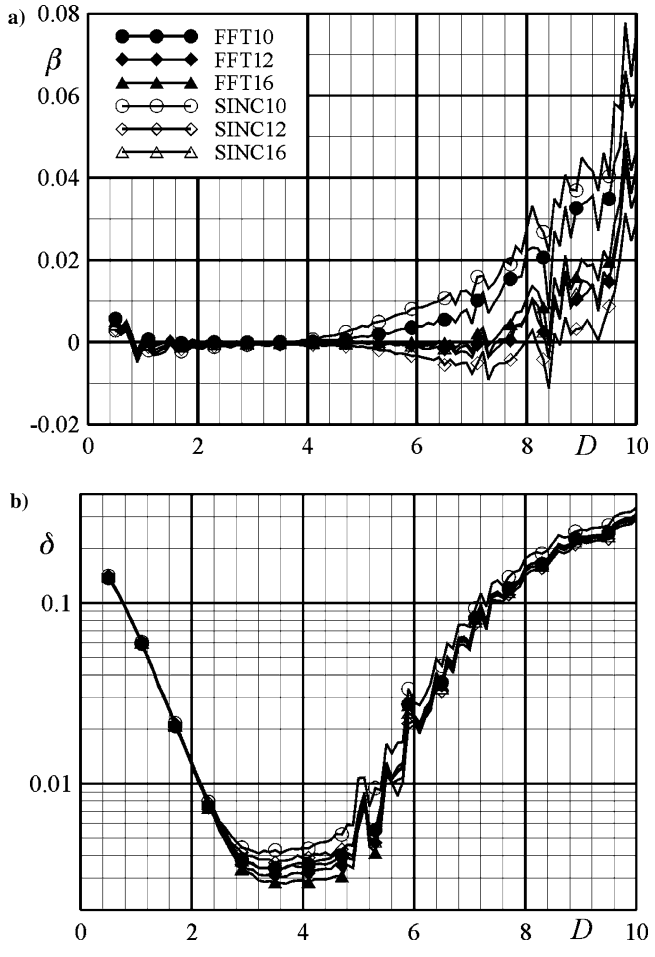

Fig. 12. Bias (**a**) and total (**b**) errors as a function of particle diameter for various IS

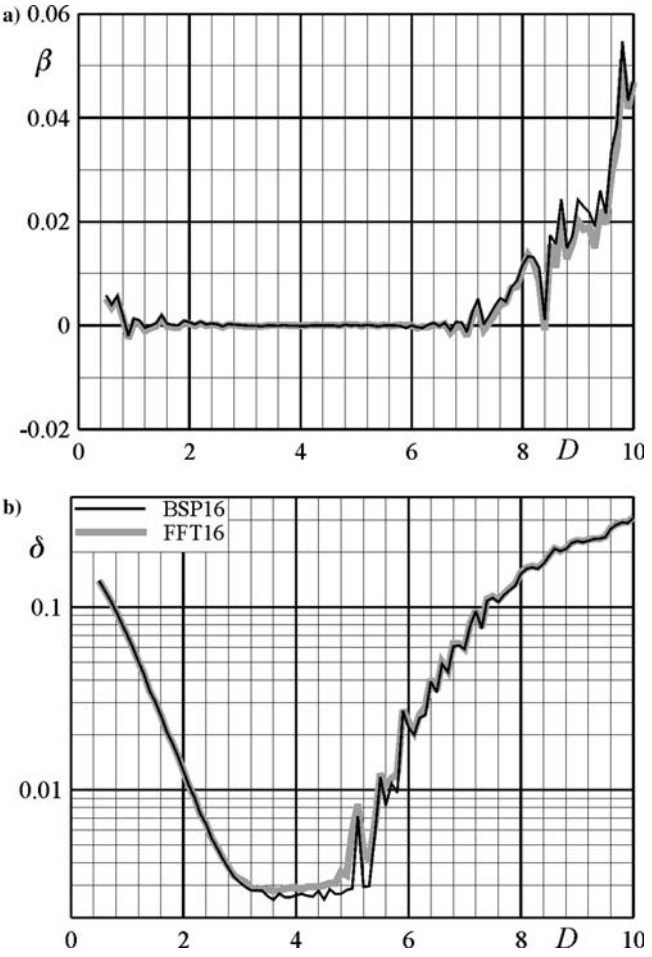

Fig. 13. Bias (**a**) and total (**b**) errors as a function of particle diameter for BSPL16 and FFT16 interpolation schemes

been examined. The total and bias errors have been analysed and, when possible, compared with results already present in the literature. The performance assessment has been conducted using synthetic images with particles of Gaussian shape, a constant displacement field and without added noise apart from the 8 bits digitalization. In this paper no attempt has been made to study the influence of the IS on the spatial resolution of the PIV algorithm and most probably this will be the object of a future work. Results show that both the systematic and total errors are strongly influenced by the interpolation scheme used in the reconstruction of the deformed images.

The choice of interpolation scheme has been proved to be a crucial point in the IDM, in fact, both the bias and total errors of image deformation methods may be even higher than that relative to classical IDWO methods. Normally, interpolation schemes, apart from B-spline, based on even linear dimensions of the interpolation grid behave significantly better than those based on odd ones.

For a particle diameter of about three pixels, when using a significant amount of interpolation points, the interpolation schemes based on the shift theorem of the Fourier transforms and B-spline result in the lowest total error and practically no bias error. The IS based on the sinc formula perform slightly worse while the schemes based on 16 or less interpolation points perform significantly worse.

The influence of particle diameter on accuracy has shown a behaviour similar to that of the classical methods. An absolute minimum is found for relatively large particle diameters and the errors increase significantly for very large and very small particles.

By also taking into account the time performances of the various IS the following conclusions may be drawn. If speed is a prime concern, simplex or bicubic methods should be used to obtain a good compromise between speed and accuracy with the former method behaving better in both the aspects. If accuracy is the only concern, the SINC, FFT or BSPL IS with a large number of points should be used which results in significantly smaller errors than that associated with the simplex method; on the other hand, the processing time may increase more than one order of magnitude. It has to be stressed that for highly overlapped final interrogation windows the time to perform the correlations may be of the same order of magnitude or, in some cases, even higher than the one needed to perform the image deformation so that even when time is a prime concern the sinc, Fourier shift theorem or B-spline based interpolation schemes may be the optimal choice.

References

Gui L, Wereley ST (2002) A correlation-based continuous window-shift technique to reduce the peak-locking effect in digital PIV image evaluation. Exp Fluids 32:506–517

Hart DP (2000) Super-resolution PIV by recursive local-correlation. J Visual 3(2):187–194

Huang HT, Fiedler HE, Wang JJ (1993) Limitation and improvement of PIV, part 2. Particle image distortion, a novel technique. Exp Fluids 15:263–273

Jambunathan K, Ju XY, Dobbins BN, Ashforth-Frost S (1995) An improved cross correlation technique for particle image velocimetry. Meas Sci Technol 6:507–514

Keane RD, Adrian RJ (1993) Theory of cross correlation analysis of PIV images. In: Nieuwstadt FTM (ed) Flow visualization and image analysis. pp 1–25

Lecordier B, Demare D, Vervisch LMJ, Rèveillon J, Trinitè M (2001) Estimation of the accuracy of PIV treatments for turbulent flow studies by direct numerical simulation of multi-phase flow. Meas Sci Technol 12:1382–1391

Meunier P, Leweke T (2003) Analysis and treatment of errors due to high velocity gradients in particle image velocimetry. Exp Fluids 35:408–421

Nogueira J, Lecuona A, Rodriguez PA (1999) Local field correction PIV: on the increase of accuracy of digital PIV systems. Exp Fluids 27:107–116

Nogueira J, Lecuona A, Rodriguez PA (2001) Local field correction PIV, implemented by means of simple algorithms, and multigrid versions. Meas Sci Technol 12:1911–1921

Raffel M, Willert CE, Kompenhans J (1998) Particle image velocimetry: a practical guide. Springer, Berlin Heidelberg New York

Scarano F (2002) Iterative image deformation methods in PIV. Meas Sci Technol 13:R1–R19

Scarano F (2004) A super-resolution particle image velocimetry interrogation approach by means of velocity second derivatives correlation. Meas Sci Technol 15:475–486

Scarano F, Riethmuller ML (1999) Iterative multigrid approach in PIV image processing with discrete window offset. Exp Fluids 26:513–523

Scarano F, Riethmuller ML (2000) Advances in iterative multigrid PIV image processing. Exp Fluids S51–S60

Soria J (1996) An investigation of the near wake of a circular cylinder using a video-based digital cross-correlation particle image velocimetry technique. Exp Therm Fluid Sci 12:221–233

Unser M (1999) Splines: a perfect fit for signal and image processing. IEEE Signal Proc Mag 16(6):22–38

Unser M, Aldroubi A, Eden M (1993a) B-spline signal processing: part I—theory. IEEE T Signal Proces 41(2):821–832

Unser M, Aldroubi A, Eden M (1993b) B-spline signal processing: part II—efficient design and applications. IEEE T Signal Proces 41(2):834–848

Utami T, Blackwelder RF, Ueno T (1991) A cross-correlation technique for velocity field extraction from particulate visualization. Exp Fluids 10:213–223

Wereley ST, Meinhart CD (2001) Second-order accurate particle image velocimetry. Exp Fluids 31:258–268

Westerweel J (1993) Digital particle image velocimetry—theory and applications. PhD Thesis, Delft University of Technology, The Netherlands

Westerweel J (2000) Theoretical analysis of the measurement precision in particle image velocimetry. Exp Fluids 29:S3–S12

Westerweel J, Dabiri D, Gharib M (1997) The effect of a discrete window offset on the accuracy of cross-correlation analysis of digital PIV recordings. Exp Fluids 23:20–28

Willert CE, Gharib M (1991) Digital particle image velocimetry. Exp Fluids 10:181–193

Yaroslavsky LP (1996) Signal sinc-interpolation: a fast computer algorithm. Bioimaging 4:225–231